Inorg. Chem. **2008**, *47*, 6990−7001

New Palladium(II) and Platinum(II) Complexes with 9-Aminoacridine: Structures, Luminiscence, Theoretical Calculations, and Antitumor Activity

José Ruiz,*,† Julia Lorenzo,‡ Consuelo Vicente,† Gregorio López,† José María López-de-Luzuriaga,§ Miguel Monge,§ Francesc X. Avilés,‡ Delia Bautista,|| Virtudes Moreno,⊥ and Antonio Laguna*,#

Departamento de Química Inorgánica, Universidad de Murcia, E-30071 Murcia, Spain, Institut de Biotecnología i Biomedicina, Universitat Autònoma de Barcelona, E-08193 Barcelona, Spain, Departamento de Química, Universidad de La Rioja, E-26004 Logroño, Spain, SAI, Universidad de Murcia, E-30100 Murcia, Spain, Departament de Química Inorgànica, Universitat de Barcelona, E-08028 Barcelona, Spain, and Departamento de Química Inorgánica, Instituto de Ciencia de Materiales de Aragón Universidad de Zaragoza-CSIC, E-50009 Zaragoza, Spain

Received April 3, 2008

The new complexes [Pd(dmba)(*N10*-9AA)(PPh_3)]ClO_4 (**1**), [Pt(dmba)(*N9*-9AA)(PPh_3)]ClO_4 (**2**), [Pd(dmba)(*N10*-9AA)Cl] (**3**), and [Pd(C_6F_5)(*N10*-9AA)(PPh_3)Cl] (**4**) (9-AA = 9-aminoacridine; dmba = N,C-chelating 2-(dimethylaminomethyl)phenyl) have been prepared. The crystal structures have been established by X-ray diffraction. In complex **2**, an anagostic C−H···Pt interaction is observed. All complexes are luminescent in the solid state at room temperature, showing important differences between the palladium and platinum complexes. Complex **2** shows two structured emission bands at high and low energies in the solid state, and the lifetimes are in agreement with excited states of triplet parentage. Density functional theory and time-dependent density functional theory calculations for complex **2** have been done. Values of IC_{50} were also calculated for the new complexes **1**−**4** against the tumor cell line HL-60. All of the new complexes were more active than cisplatin (up to 30-fold in some cases). The DNA adduct formation of the new complexes synthesized was followed by circular dichroism and electrophoretic mobility. Atomic force microscopy images of the modifications caused by the complexes on plasmid DNA pB*R*322 were also obtained.

Introduction

Acridine is an aza-aromatic compound, and its derivatives have been widely used in pharmacology.[1,2] Its polyaromatic nature facilitates the intercalation between DNA base pairs.[1] The 9-aminoacridine (9-AA) molecule has two symmetrically distributed nitrogen atoms with nucleophilic properties: the exocyclic N(9) and the endocyclic N(10). Two tautomeric forms of the free 9-aminoacridine moiety can be adopted in solution (see Scheme 1).

Scheme 1. Schematic Representation of the Two Tautomeric Forms of the 9-Aminoacridine

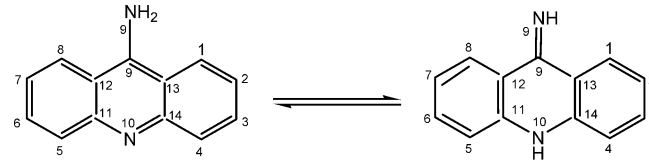

To the best of our knowledge,[3] there are no examples of 9-aminoacridine metal complexes where the ligand is coordinated in its amine form, bound to the metal atom in a monodentate fashion by the endocyclic nitrogen atom, and

* Authors to whom correspondence should be addressed. E-mail: jruiz@um.es (J.R.); alaguna@unizar.es (A.L.).
† Departamento de Química Inorgánica, Universidad de Murcia.
‡ Institut de Biotecnología i Biomedicina, Universitat Autònoma de Barcelona.
§ Departamento de Química, Universidad de La Rioja.
|| SAI, Universidad de Murcia.
⊥ Departament de Química Inorgànica, Universitat de Barcelona.
Instituto de Ciencia de Materiales de Aragón Universidad de Zaragoza.

(1) Farrell, N. *Transition Metal Complexes as Drugs and Chemotherapeutic Agents*; Kluwer Academic Publishers: Dordrecht, The Netherlands, 1989.
(2) Korth, C.; May, B. C. H.; Cohen, F. E.; Prusiner, S. B. *Proc. Natl. Acad. Sci. U. S. A.* **2001**, *98*, 9836–9841.
(3) *CCDC CSD*, version 5.28, November 2006, update May 2007.

10.1021/ic800589m CCC: $40.75
Published on Web 07/01/2008

Scheme 2

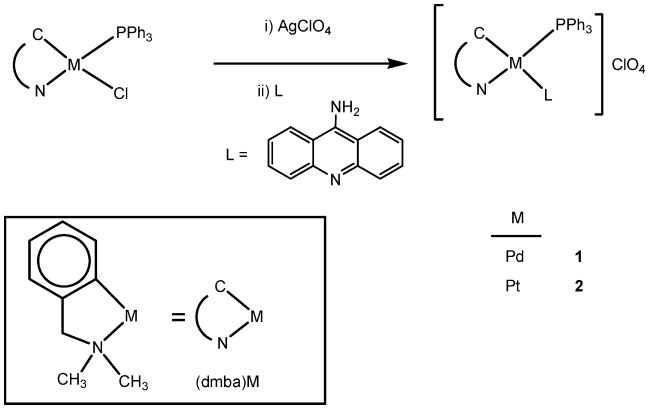

only two examples, reported by Lippard et al.,[4] where the ligand is coordinated in its imine form, which binds to the metal atom in a monodentate fashion by the exocyclic nitrogen atom: *cis*-[Pt(NH_3)$_2$(*N9*-9-AA)Cl](NO_3) and *cis*-[Pt(NH_3)$_2$(*N9*-9-AA)$_2$](NO_3)$_2$. Metalations of 9-aminoacridine and nitro-9-[(2-aminoethyl)amino]acridines have been also reported.[5–7] The interaction of 9-aminoacridinecarboxamide platinum complexes with DNA has been investigated.[8] Moreover, platinum−acridinylthiourea conjugates are a new class of cytotoxic DNA-targeted agents that act through a hybrid mechanism involving monofunctional platination of nucleobase nitrogen and classical intercalation.[9–11] On the other hand, the excitation spectra for 9-aminoacridine and some platinum and ruthenium derivatives have been reported.[12,13]

In this work, we describe the syntheses, structures, and luminescent properties of new 9-aminoacridine palladium and platinum derivatives from the N,C-chelating 2-(dimethylaminomethyl)phenyl (dmba) and pentafluorophenyl C_6F_5 groups. Density functional theory (DFT) and time-dependent density functional theory (TD-DFT) calculations are reported. To our knowledge, the structures of complexes [Pd(dmba)(*N10*-9AA)(PPh_3)]ClO_4, [Pd(dmba)(*N10*-9AA)Cl], and [Pd(C_6F_5)(*N10*-9AA)(PPh_3)Cl] represent the first examples of metal complexes where the ligand 9-AA is coordinated in a monodentate fashion by the endocyclic nitrogen atom. The in vitro antiproliferative activity of the new complexes in the HL-60 cell line has also been studied. All of the new complexes were more active than cisplatin (up to 30-fold in some cases).

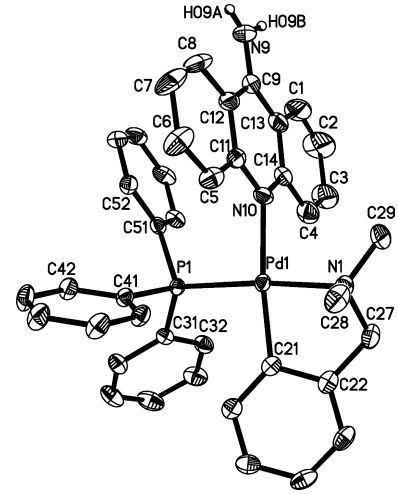

Figure 1. ORTEP representation (50% probability) of **1**. Selected bond lengths (Å) and angles (deg): Pd(1)−C(21) = 2.011(3), Pd(1)−N(10) = 2.121(6), Pd(1)−N(1) = 2.139(2), Pd(1)−P(1) = 2.2579(7), C(21)−Pd(1)−N(10) = 173.51(19), C(21)−Pd(1)−N(1) = 81.14(10), N(10)−Pd(1)−N(1) = 94.03(18), C(21)−Pd(1)−P(1) = 93.85(8), N(10)−Pd(1)−P(1) = 91.40(16), N(1)−Pd(1)−P(1) = 172.10(7).

Results and Discussion

Syntheses and Structures of [M(dmba)(PPh_3)(9-AA)]ClO_4. The dmba complexes [Pd(dmba)(PPh_3)(*N10*-9-AA)]ClO_4 (**1**) and [Pt(dmba)(PPh_3)(*N9*-9-AA)]ClO_4·acetone (**2**) have been prepared from the corresponding chlorometal complex [M(dmba)(PPh_3)Cl] (M = Pd or Pt). After precipitation of AgCl by the addition of $AgClO_4$ in a 1:1 molar ratio in acetone, the solvent complexes [M(dmba)(PPh_3)(Me_2CO)]ClO_4 (M = Pd or Pt), generated in situ, react with 1 equiv of 9-AA to give the cationic complexes [M(dmba)(PPh_3)(9-AA)]ClO_4 (**1** and **2**) (Scheme 2).

Complexes **1** and **2**·acetone are yellow, air-stable solids that decompose upon heating above 180 °C in a dynamic N_2 atmosphere. An IR band is observed at ca. 1095, which is assigned to the ν_3 mode of free perchlorate (T_d symmetry). The observation of an additional band at ca. 623 cm^{-1} for the ν_4 mode confirms the presence of free perchlorate.[14]

Complexes **1** and **2**·acetone were isolated as single crystals suitable for X-ray diffraction studies following procedures described in the Experimental Section. The crystal structure of compound **1** consists of mononuclear [Pd(dmba)(PPh_3)(*N10*-9-AA)]$^+$ cations (Figure 1) and perchlorate anions. The acridine ligand 9-AA is coordinated in a monodentate fashion by the endocyclic nitrogen atom N(10), no examples of this type of coordination mode being previously reported.[3] The palladium coordination geometry is approximately square-planar, although the angles around palladium deviate from 90° due to the bite of the cyclometallated ligand. The acridine ring is nearly perpendicular to the Pd square plane. The

(4) Sundquist, W. I.; Bancroft, D. P.; Lippard, S. J. *J. Am. Chem. Soc.* **1990**, *112*, 1590–1596.
(5) Ceci, E.; Cini, R.; Konopa, J.; Maresca, L.; Natile, G. *Inorg. Chem.* **1996**, *35*, 876–882.
(6) Riera, X.; Moreno, V.; Ciudad, C. J.; Noe, V.; Font-Bardía, M.; Solans, X. *Bioinorg. Chem. Appl.* **2007**, 2007; Article ID 98732, 15 pages, DOI:, 10.1155/2007/98732.
(7) Maresca, L.; Pacifico, C.; Pappadopoli, M. C.; Natile, G. *Inorg. Chim. Acta* **2000**, *304*, 274–282.
(8) Temple, M. D.; McFadyen, W. D.; Holmes, R. J.; Denny, W. A.; Murray, V. *Biochemistry* **2000**, *39*, 5593–5599.
(9) Guddneppanavar, R.; Choudhury, J. R.; Kheradi, A. R.; Steen, B. D.; Saluta, G.; Kucera, G. L.; Day, C. S.; Bierbach, U. J. *Med. Chem.* **2007**, *50*, 2259–2263.
(10) Baruah, H.; Rector, C. L.; Monnier, S. M.; Bierbach, U. *Biochem. Pharmacol.* **2002**, *64*, 191–200.
(11) Baruah, H.; Barry, C. G.; Bierbach, U. *Curr. Top. Med. Chem.* **2004**, *4*, 1537–1549.
(12) de Carvalho, I. M. M.; Moreira, I. D.; Gehlen, M. H. *Inorg. Chem.* **2003**, *42*, 1525–1531.
(13) Scolaro, L. M.; Alibrandi, G.; Romeo, R.; Ricevuto, V.; Campagna, S. *Inorg. Chem.* **1992**, *31*, 2074–2078.
(14) Nakamoto, K. *Infrared and Raman Spectra of Inorganic and Coordination Compounds*, 5th ed.; Wiley-Interscience: New York, 1997; p 199.

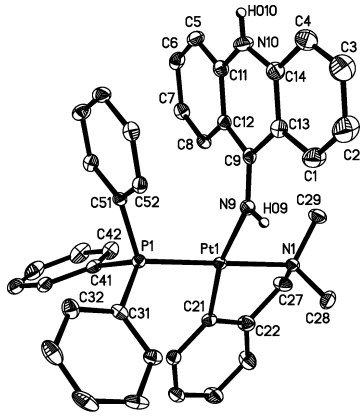

Figure 2. ORTEP representation (50% probability) of **2**·acetone. Selected bond lengths (Å) and angles (deg): Pt(1)−C(21) = 2.015(3), Pt(1)−N(9) = 2.096(3), Pt(1)−N(1) = 2.137(3), Pt(1)−P(1) = 2.2315(8), C(21)−Pt(1)−N(9) = 167.97(12), C(21)−Pt(1)−N(1) = 81.61(12), N(9)−Pt(1)−N(1) = 89.37(11), C(21)−Pt(1)−P(1) = 96.07(9), N(9)−Pt(1)−P(1) = 93.35(8), N(1)−Pt(1)−P(1) = 176.15(8).

complex shows extensive intermolecular N−H···O and C−H···O bond links between the palladium ligands and perchlorate counterions. Intermolecular aromatic CH/π interactions[15] are also found.

The structure of **2**·acetone consists of mononuclear [Pt(dmba)(PPh_3)(*N9*-9-AA)]$^+$ cations and perchlorate anions. The cation of **2**·acetone is depicted in Figure 2. In contrast to complex **1**, here, the acridine ligand adopts an imino-type configuration with the proton of the exocyclic 9-amino group shifted on N(10), being N(9) and N(10) sp^2-hybridized, as was previously observed in the related complex *cis*-[Pt(NH_3)$_2$(*N9*-9-AA)Cl](NO_3).[4]

The C(9)−N(9) bond distance [1.305(4) Å] is quite short, and the value is very close to the mean value reported for free acridines in the imino tautomeric configuration.[5] The asymmetric coordination of 9-aminoacridine in this complex renders the acridine ring protons inequivalent and brings the H(8) atoms close to the platinum atom, with a Pt···H(8) distance of 2.539 Å and a Pt···H(8)−C(8) angle of 143(12)°, which clearly indicates the presence of an anagostic interaction.[16,17]

The acridine moiety is nearly perpendicular to the Pt square plane (average dihedral angle, 75.73°) and is folded about the C(9)−N(10) vector with an average angle between outer rings of 8.99°. The C(21)−Pt−N(1) angle of 81.61(12)° is within the normal range for such dmba metal complexes.[18–22] The PPh_3 ligand is trans to the nitrogen donor, displaying no tendency to occupy the position trans to the σ-bound orthoplatinated aryl group.[23] Furthermore, there is an intramolecular interaction by phenyl-AA π-stacking (centroid−centroid distance: 3.654 Å).[24,25] The complex also shows extensive intermolecular N−H···O and C−H···O bond links between the platinum ligands, perchlorate counterions, and lattice acetone molecules. In particular, the imino proton on the acridine N(10) position is stabilized by

Scheme 3

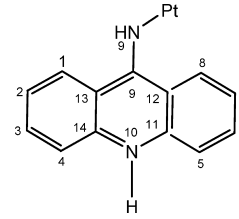

hydrogen-bonding interactions with the perchlorate anion. Intermolecular aromatic CH/π interactions[15] are also found [distance H36···centroid (C5,C6,C7,C8,C11,C12): 2.583 Å].

The ^{1}H and ^{13}C NMR spectra in acetone-d_6 of complexes **1** and **2**·acetone at room temperature are quite different (see the Experimental Section), indicating that in solution the amine tautomeric form of 9-AA is present in complex **1**, whereas the imine tautomeric form is observed in complex **2**·acetone, as it also occurs in the solid state (Figures 1 and 2). Thus, for complex **1**, a unique set of four resonances is observed for the aromatic resonances of AA in a 2:2:2:2 ratio. The observation at 25 °C of the NCH_2 and NMe_2 proton signals as doublets (due to phosphorus coupling) suggests that the inversion of the configuration at the PdCCCN chelate ring is faster than the NMR time scale.[18,26] Broad resonances are observed at room temperature for the NH_2 group and the PPh_3 protons, the PPh_3 proton resonances becoming sharp at −60 °C and +50 °C. No other significant changes are observed in the variable-temperature ^{1}H NMR spectra of complex **1**. The assignments given in the Experimental Section for complex **1** were supported by the pertinent heteronuclear (^{1}H−^{13}C) correlation spectroscopy (COSY) technique.

On the other hand, for complex **2**·acetone, NMR spectroscopic studies demonstrated the persistence of the asymmetric imino coordination of 9-AA in acetone-d_6 solutions of the complex **2**·acetone at 25 °C (Scheme 3). No significant changes are observed in the ^{1}H NMR spectra over the −60° to +50 °C range. The ^{1}H spectra for **2**·acetone were assigned as follows (for the numbering scheme, see Scheme 3): the proton resonance at very low field was assigned as H8 on the basis of the crystal structure of **2**·acetone, which reveals the unique location of this proton above the platinum square plane, the short Pt−H8 distances resulting in paramagnetic deshielding of the H8 protons by approximately 2.64 ppm versus aminoacridine free base. Protons H7, H6, and H5 could then be assigned from the connectivity observed in a COSY spectrum. As shown by ^{1}H NMR, protons on H9 and

(15) Nishio, M. *CrystEngComm* **2004**, *6*, 130–158.
(16) Braga, D.; Grepioni, F.; Tedesco, E.; Biradha, K.; Desiraju, G. R. *Organometallics* **1997**, *16*, 1846–1856.
(17) Brookhart, M.; Green, M. L. H.; Parkin, G. *PNAS* **2007**, *104*, 6908–6914.
(18) Ruiz, J.; Cutillas, N.; Rodríguez, V.; Sampedro, J.; López, G.; Chaloner, P. A.; Hitchcock, P. B. *J. Chem. Soc., Dalton Trans.* **1999**, 2939–2946.
(19) Bedford, R. B.; Cazin, C. S. J.; Coles, S. J.; Gelbrich, T.; Horton, P. N.; Hursthouse, M. B.; Light, M. E. *Organometallics* **2003**, *22*, 987–999.
(20) Ruiz, J.; Cutillas, N.; López, F.; López, G.; Bautista, D. *Organometallics* **2006**, *25*, 5768–5773.
(21) Dupont, J.; Pfeffer, M.; Spencer, J. *Eur. J. Inorg. Chem.* **2001**, 1917–1927.
(22) Ruiz, J.; Villa, M. D.; Cutillas, N.; López, G.; de Haro, C.; Bautista, D.; Moreno, V.; Valencia, L. *Inorg. Chem.* **2008**, *47*, 4490–4505.
(23) Otto, S.; Samuleev, P. V.; Polyakov, V. A.; Ryabov, A. D.; Elding, L. I. *Dalton Trans.* **2004**, 3662–3668.

Scheme 4

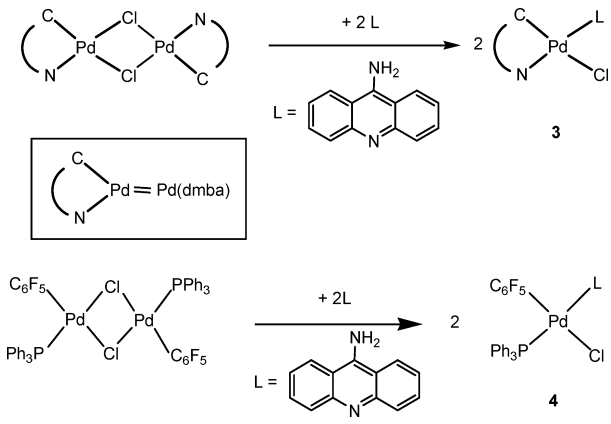

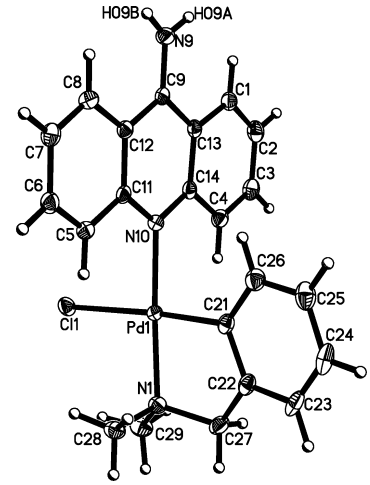

Figure 3. ORTEP representation (50% probability) of **3**·DMF. Selected bond lengths (Å) and angles (deg): Pd(1)−C(21) = 1.983(2), Pd(1)−N(10) = 2.0541(17), Pt(1)−N(1) = 2.0913(18), Pd(1)−Cl(1) = 2.4297(5), C(21)−Pd(1)−N(10) = 91.92(8), C(21)−Pd(1)−N(1) = 82.97(8), N(10)−Pd(1)−N(1)=174.30(7),C(21)−Pd(1)−Cl(1)=173.57(6),N(10)−Pd(1)−Cl(1) = 90.89(5), N(1)−Pd(1)−Cl(1) = 93.93(5).

Table 1. Hydrogen Bonds [Å and deg] for Complex **3**·DMF

D−H···A	*d*(D−H)	*d*(H···A)	*d*(D···A)	<(DHA)
C(91)−H(91)···Cl(1)	0.96(3)	2.90(3)	3.786(2)	155(2)
N(9)−H(09B)···O(1)#1	0.89(3)	1.99(3)	2.839(3)	161(3)
N(9)−H(09A)···Cl(1)#1	0.83(3)	2.46(3)	3.254(2)	161(2)
C(1)−H(1)···Cl(1)#1	0.95	2.86	3.777(2)	162.5
C(8)−H(8)···O(1)#1	0.95	2.51	3.439(3)	166.1
C(6)−H(6)···Cl(1)#2	0.95	2.86	3.761(2)	158.4
C(93)−H(93B)···Cl(1)#3	0.98	2.86	3.623(3)	135.4

H10 of the imino 9-AA of complex **2**·acetone were observed directly in acetone-d_6 solution at 9.16 and 10.6 ppm, respectively. Selective irradiation of the H9 resonance resulted in a strong nuclear Overhauser enhancement (NOE) of the H8 (16%), but not the H1 resonance (Scheme 3). Selective irradiation of the H10 resonance resulted in a NOE (4%) of both the H4 and H5 resonances, as expected. The ^{1}H NMR spectrum shows also that both the N*Me*$_2$ and the *CH*$_2$N group of the dmba are diastereotopic, two separate signals being observed for the former (coupled to ^{31}P) and an AB quartet for the latter (the resonance at δ 4.22 appears as a doublet of doublets, due also to ^{31}P coupling). Therefore, there is no plane of symmetry in the palladium coordination plane.

Syntheses and Structures of [Pd(dmba)(9-AA)(Cl)] and [Pd(C_6F_5)(9-AA)(Cl)]. The ready reaction of [Pd(dmba)(μ-Cl)]$_2$ and [Pd(C_6F_5)(PPh_3)(μ-Cl)]$_2$ in $CHCl_3$ with 9-AA in a 1:2 molar ratio gives mononuclear complexes **3** and **4**, respectively (Scheme 4).

The complexes are air-stable, both in the solid state and in solution, and they are yellow. In the far-IR spectra of complexes **3** and **4** is exhibited a band assigned to ν(Pd−Cl) at 358 cm^{-1} (for **3**) and 298 cm^{-1} (for **4**). In the zone between 1670 and 1550 cm^{-1}, the stretching ν(>C═N−) and bending $\delta(NH_2)$ bands can be assigned. The $\delta(NH_2)$ band of the free ligand appears at 1670 cm^{-1}. The IR spectrum of complex **4** shows also an absorption at 783 cm^{-1} that is observed as a single band for the so-called X-sensitive mode,[27] as expected from the presence of only one C_6F_5 group in the coordination sphere of the palladium atom. In the IR spectra of compound **4**, the form of the bands between 550 and 520 cm^{-1}, corresponding to the triphenylphosphine molecules, confirms the coordination of the palladium atom to only one molecule of PPh_3.

The structure of complex **3**·DMF is shown in Figure 3. The acridine ligand 9-AA is coordinated in a monodentate fashion by the endocyclic nitrogen atom N(10) and is planar (average angle between outer rings of 1.47°). The Cl ligand is trans to the carbon donor, as found in related complexes of the type [Pd(dmba)Cl(L)] (L = py,[28,29] PTA,[22] or PPh_3[29]), the Pd−Cl bond length being rather long, consistent with the large ground-state trans influence of the σ-bound carbon atom.[23] The acridine ring is nearly perpendicular to the Pd square plane (average dihedral angle, 85.32°). The complex also shows extensive intermolecular N−H···O, C−H···O, N−H···Cl, and C−H···Cl bond links between the palladium ligands and lattice DMF molecules (Table 1). Furthermore, there is an intermolecular interaction by DMF-AA π-stacking (distance N(4)···centroid (C5,C6,C7,C8,C11,C12): 3.592 Å and O(1)···centroid (C9−C14): 3.337 Å).

The structure of complex **4**·acetone·toluene is shown in Figure 4. The palladium atom is in a slightly distorted square-planar geometry. The acridine ligand 9-AA is coordinated by the endocyclic nitrogen atom N(10) and is planar, the Pd(1)−N(10) (2.1201 Å) being longer than that found in complex **3**·DMF (2.0541 Å). The Pd−C_6F_5 bond length is in the range found in the literature for pentafluorophenyl complexes.[30–34]

(24) Janiak, C. *J. Chem. Soc., Dalton Trans.* **2000**, 3885–3896.
(25) Ruiz, J.; Lorenzo, J.; Sanglas, L.; Cutillas, N.; Vicente, C.; Villa, M. D.; Avilés, F. X.; López, G.; Moreno, V.; Pérez, J.; Bautista, D. *Inorg. Chem.* **2006**, *45*, 6347–6360.
(26) Ruiz, J.; Rodríguez, V.; Cutillas, N.; López, G.; Pérez, J. *Organometallics* **2002**, *21*, 4912–4918.
(27) Maslowski, E. *Vibrational Spectra of Organometallic Compounds*; Wiley: New York, 1977; p 437.
(28) Lu, Z. L.; Neverov, A. A.; Brown, R. S. *Org. Biomol. Chem.* **2005**, *3*, 3379–3387.
(29) Mentes, A.; Kemmitt, R. D. W.; Fawcett, J.; Russell, D. R. *J. Mol. Struct.* **2004**, *693*, 241–246.
(30) Althoff, G.; Ruiz, J.; Rodríguez, V.; López, G.; Pérez, J.; Janiak, C. *CrystEngComm* **2006**, *8*, 662–665.
(31) Forniés, J.; Martínez, F.; Navarro, R.; Urriolabeitia, E. P. *J. Organomet. Chem.* **1995**, *495*, 185–194.

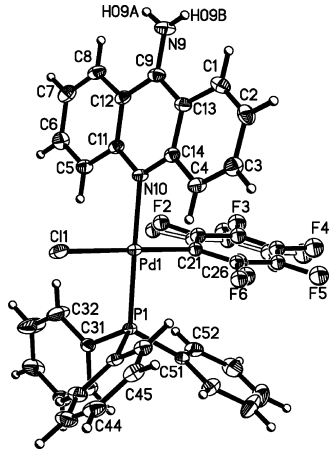

Figure 4. ORTEP representation (50% probability) of **4**·acetone·toluene. Selected bond lengths (Å) and angles (deg): Pd(1)−C(21) = 1.974(7), Pd(1)−C(21′)= 2.050(8), Pd(1)−N(10) = 2.1201(18), Pd(1)−P(1) = 2.2518(6), Pd(1)−Cl(1) = 2.3629(6), C(21)−Pd(1)−C(21′) = 6.5(3), C(21)−Pd(1)−N(10) = 88.1(2), C(21′)−Pd(1)−N(10) = 89.3(2), C(21)−Pd(1)−P(1) = 91.29(19), C(21′)−Pd(1)−P(1) = 90.2(2), N(10)−Pd(1)−P(1) = 178.64(5), C(21)−Pd(1)−Cl(1) = 178.0(2), C(21′)−Pd(1)−Cl(1) = 175.4(2), N(10)−Pd(1)−Cl(1) = 92.16(5), Cl(1)−Pd(1)−P(1) = 88.38(2).

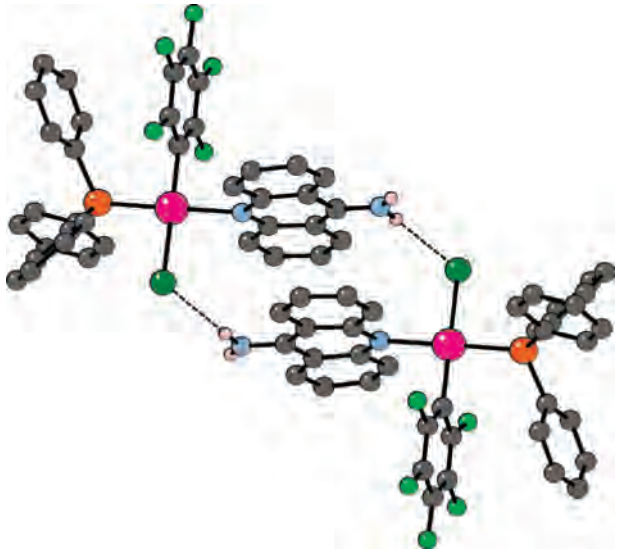

Figure 5. The dimeric structure of complex **4**·acetone·toluene, showing the hydrogen bonds.

An interesting feature of the crystal structure is the presence of dimeric units of $[Pd(C_6F_5)(N10\text{-}9AA)(PPh_3)Cl]_2$ due mainly to the intermolecular NH···Cl hydrogen bond (Figure 5). A stacking interaction between AA pairs is also present, which may result in synergism with the observed N−H···Cl H-bonding interaction to favor the supramolecular association. It is noteworthy that the intramolecular π-interaction appears between the electron-poor C_6F_5 ring and a phenyl ring of the phosphine, showing a rather short centroid−centroid contact (Ct···Ct < 3.8 Å),[30] although the ring planes are not coplanar. The C_6F_5 ring is surrounded by C−H moieties from phenyl rings, and intermolecular interaction contacts C−H···F−C are observed.[30,35]

The ^{1}H and ^{13}C NMR spectra in DMSO-d_6 of complexes **3**·$CHCl_3$ and **4**·$^1/_2CHCl_3$ indicate that in solution the amine tautomeric form of 9-AA is present in both complexes. The ^{19}F NMR spectrum of **4**·$^1/_2CHCl_3$ in solution, at room temperatue, shows a unique set of sharp resonances, indicating the presence of only one type of C_6F_5 group.

Luminescence Studies on Complexes 1−4. All complexes are luminescent in the solid state at room temperature, showing important differences between the palladium and platinum complexes. As we have seen, from a structural viewpoint, the main difference is that, in the platinum complex **2**·acetone, the 9-AA ligand is bonded to the metal center in a zwitterionic (acridinium) form, whereas in the palladium complexes, the amino form of the 9-AA ligand is present.[4] Thus, complexes **1**, **3**·$CHCl_3$, and **4**·$^1/_2CHCl_3$ display high-energy structured emissions at 490 nm (exc. 400 nm), 500 nm (exc. 400 nm), and 505 nm (exc. 400 nm), respectively. This high-energy structured emission at ca. 500 nm observed for all the palladium complexes is similar to that displayed by the free 9-AA ligand.[36] By contrast, the platinum complex **2**·acetone shows, under the same conditions, two structured emission bands at high energy (492 nm, exc. 450 nm) and low energy (602 nm, exc. 350 nm).

All complexes are also luminescent in 5×10^{-4} M CH_2Cl_2 solutions at room temperature, showing only high-energy emissions at ca. 500 nm. In the case of the low-energy emission for complex **2**·acetone, it appears when the temperature is decreased to 77 K (Figure 7).

We have studied in detail the photoluminescent properties of platinum complex **2**. The lifetimes of both emissions observed for complex **2**·acetone are quite different, that of the high-energy emission being ca. 10 μs, whereas that of the low-energy emission is ca. 1.25 ms. These lifetimes are in agreement with excited states of triplet parentage.

The excitation spectrum of this complex shows that a high-energy excitation favors the low-energy emission and that a low-energy excitation favors the high-energy emission (see Figure 6). Since both emissions are obtained upon excitation at high or low energy, it can be stated that both excited states have a common energetic zone. In view of the experimental data (see below), it seems plausible that the emissions arise from intercrossed excited states of triplet parentage, since the high-energy excitation produces the low-energy emission and *vice versa* (see inset in Figure 6).

Taking into account that the structured high-energy band is similar for all complexes and also is similar to that of the 9-AA ligand, the assignment of the excited state is likely to arise from a triplet ligand (acridine)-centered (^{3}LC) excited state.

By contrast, the assignment of the low-energy emission for complex **2**·acetone is more complicated because there

(32) Ruiz, J.; Martínez, M. T.; Florenciano, F.; Rodríguez, V.; López, G.; Pérez, J.; Chaloner, P. A.; Hitchcock, P. B. *Inorg. Chem.* **2003**, *42*, 3650–3661.
(33) Ruiz, J.; Martínez, M. T.; Florenciano, F.; Rodríguez, V.; López, G.; Pérez, J.; Chaloner, P. A.; Hitchcock, P. B. *Dalton Trans.* **2004**, 929–932.
(34) Ruiz, J.; Cutillas, N.; Vicente, C.; Villa, M. D.; López, G.; Lorenzo, J.; Avilés, F. X.; Moreno, V.; Bautista, D. *Inorg. Chem.* **2005**, *44*, 7365–7376.
(35) Ruiz, J.; Villa, M. D.; Rodríguez, V.; Cutillas, N.; Vicente, C.; López, G.; Bautista, D. *Inorg. Chem.* **2007**, *46*, 5448–5449.
(36) Sandeep, P.; Bisht, P. B. *Chem. Phys.* **2006**, *326*, 521–526.

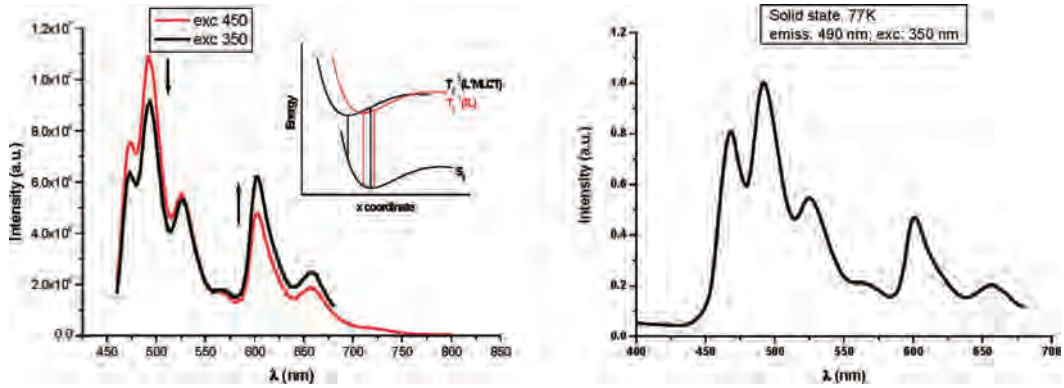

Figure 6. Emission spectra for complex **2**·acetone in the solid state at room temperature upon excitation at 450 nm (red) and 350 nm (black). (Inset) Mechanism of excitation from the ground state (S_0) to the lowest triplet excited states (T_1 and T_2) (left). Emission spectra for complex **2**·acetone in solid state at 77K (right).

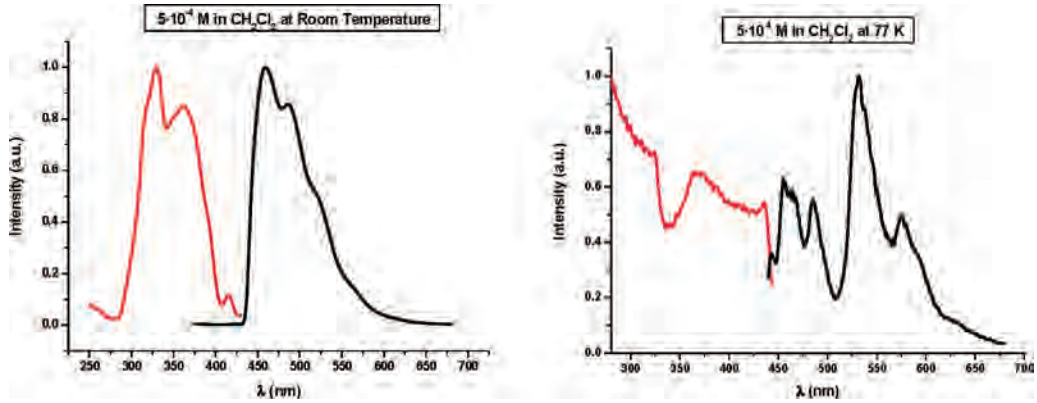

Figure 7. Excitation and emission spectra for complex **2**·acetone in 5×10^{-4} M CH_2Cl_2 solution at room temperature (left) and at 77 K (right).

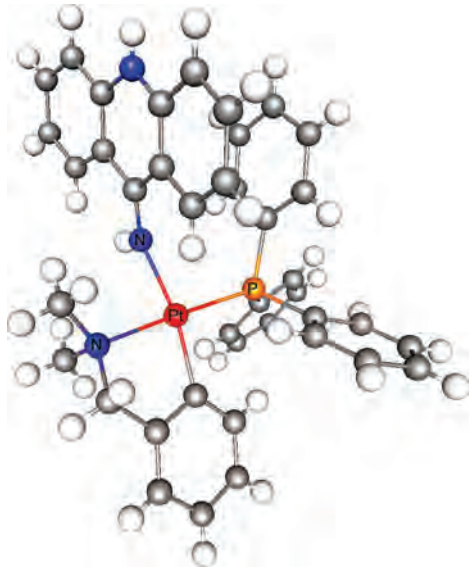

Figure 8. Theoretical model $[Pt(Acridinium)(PPh_3)(C_6H_4-CH_2NMe_2)]^+$.

are several possibilities, including triplet ligand (dmba)-centered (^{3}L′C), triplet metal-centered (^{3}MC), or triplet ligand-to-metal charge transfer (^{3}LMCT).

First, the structured profile of the low-energy emission suggests that the difference between the vibrational levels in the ground state is large. Since the emissions having a metal origin are usually unstructured and broad, this suggests that this emission is not a pure ^{3}MC transition and that the dmba ligand is, to some extent, involved.

Second, since palladium complex **1** bears the same ligands as complex **2**·acetone and does not display the low-energy emission, a possible ^{3}L′C origin of the low-energy emission can be ruled out.

Therefore, it is highly likely that the high-energy band arises from a metal-perturbed ^{3}LC excited state, and the low-energy emission arises from a ligand-metal-to-ligand charge transfer. In the case of the palladium complexes, the absence of the low-energy emission is likely to be due to a higher energy difference between the metal and ligand orbitals.

Finally, the fact that the low-energy emission is missed in solution is probably due to its very long lifetime, since the collisions between complex **2** and solvent molecules in the excited state are more effective and, therefore, the nonradiative deactivation is favored. Moreover, when the spectrum is registered in CH_2Cl_2 at 77 K, the low-energy emission is recovered because the nonradiative deactivation processes are reduced when the temperature is decreased (Figure 7).

DFT and TD-DFT Calculations. In view of the results reported in the photophysical studies section and in order to demonstrate these assumptions, single-point DFT and time-dependent DFT calculations have been carried out on a model

Scheme 5. Frontier Orbitals 164a (HOMO-1), 165a (HOMO), and 166a (LUMO)

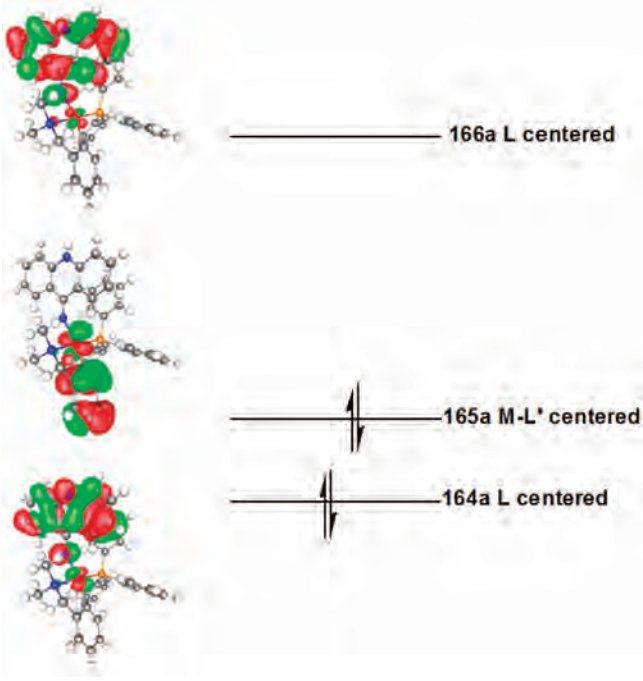

system consisting of the complete structure of the cation $[Pt(Acridinium)(PPh_3)(C_6H_4-CH_2NMe_2)]^+$ of complex **2** (Figure 8).

We have analyzed first the electronic structure of this model system obtained through single-point DFT calculations. Hence, we can check the contribution of each part of the molecule to the frontier orbitals involved in the transitions responsible for the photoluminescent properties. The most important frontier orbitals are the occupied 164a (HOMO-1) and 165a (HOMO) and the empty 166a (LUMO) (HOMO = highest occupied molecular orbital; LUMO = lowest unoccupied molecular orbital). The shape of these orbitals is given in Scheme 5. Thus, while orbital 164a is mainly located at the acridinium ligand with a small contribution from the platinum center, orbital 165a is mostly centered at the arylic ligand ($C_6H_4-CH_2NMe_2$) and the platinum center. The lower-energy empty orbital 166a (LUMO) is placed at the acridinium ligand with some contribution from the platinum center. This preliminary DFT calculation indicates that, regarding the shape of the frontier orbitals, both ligand (dmba)-metal-to-ligand (acridinium) charge transfer (L′MLCT) and ligand (acridinium)-centered transitions would be favored.

In the experimental results, the two emissions observed for complex **2** display lifetimes in the microsecond range. As we have mentioned above, these transitions can be related to triplet excited states. The use of TD-DFT calculations permits the estimation of the energies of the two lowest triplet excited states and which are the orbitals involved in each transition. The TD-DFT results confirm the anticipated tendency observed in the DFT calculations. Scheme 6 shows the orbitals involved in the two first triplet transitions. The lowest triplet transition (T_1) occurs at a theoretical value of 497 nm (exp 450 nm) between orbitals 164a and 166a. As we have commented upon before, both orbitals are mainly located at the acridinium ligand, which agrees with an internal transition in this ligand (^{3}LC). The second triplet transition (T_2) appears at a theoretical value of 424 nm (exp 350 nm) between orbitals 165a and 166a. The previous analyses of the orbitals have shown that they are located at the $(C_6H_4-CH_2NMe_2)Pt$ fragment (165a) and the acridinium ligand (166a), which suggests a triplet ligand (dmba)-metal-to-ligand (acridinium) charge transfer (^{3}L′MLCT) transition. The prediction of T_1 and T_2 excited states using TD-DFT

Scheme 6. Lowest Triplet Excitations T1 (left) and T2 (right)

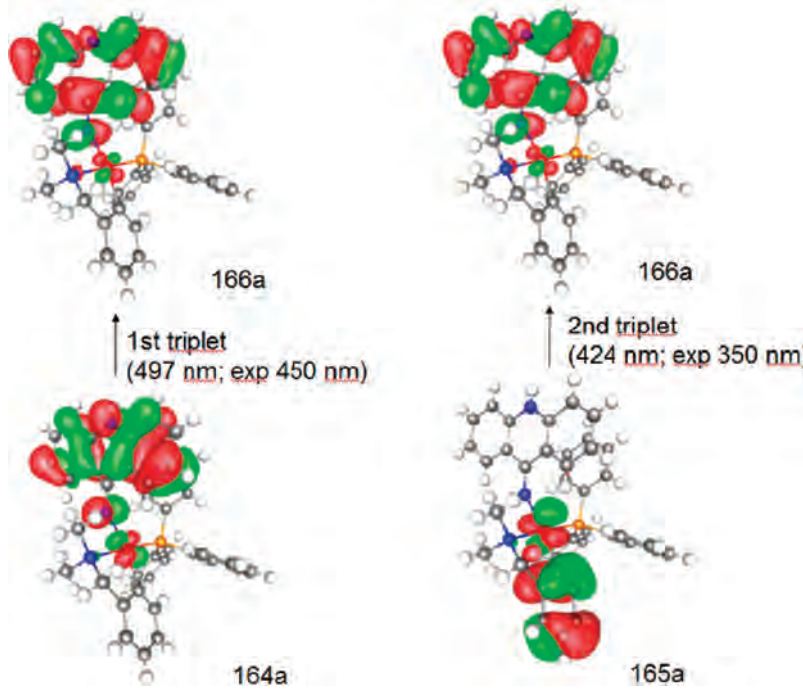

calculations is in good agreement with those obtained in the experimental results.

Biological Assays. Circular Dichroism Spectroscopy. The circular dichroism (CD) spectra of calf thymus DNA alone and incubated with compounds **1**−**4** and free 9-AA at 37 °C for 24 h with several molar ratios were recorded (Figure 9). The new metal complexes induce modifications in the secondary structure of DNA. In principle, they can interact with the DNA by intercalation of the ligand aminoacridine. Looking at the spectrum recorded for the ct-DNA incubated with the complex **3**, an increasing of the ellipticity of the positive and negative bands with increasing values of r_i ([DNA]/[complex]) can be observed.

For the complexes **1**, **2**, and **4**, an increase of the ellipticity of the bands when $r_i = 0.1$ and 0.3 is observed, and a decrease is observed when $r_i = 0.5$. All of the new complexes show a hypsochromic shift of the bands, as happens for the free classical intercalator 9-aminoacridine (9AA) (Figure 9).

Gel Electrophoresis of Compound−**pB*R*322 Complexes.** The influence of the compounds on the tertiary structure of DNA was determined by their ability to modify the electrophoretic mobility of the covalently closed circular (ccc) and open (oc) forms of pB*R*322 plasmid DNA. The platinum complexes and the free ligand 9-AA were incubated at the molar ratio $r_i = 0.5$ with pB*R*322 plasmid DNA at 37 °C for 24 h. Representative gels obtained for complexes **1**−**4** are shown in Figure 10. The behavior of the gel electrophoretic mobility of both forms, ccc and oc, of pB*R*322 plasmid and DNA/cisplatin adducts is consistent with previous reports.[37] When the pB*R*322 was incubated with complexes **1**, **3**, and **4** and the ligand 9-AA, the rate of migration of the ccc form decreased, indicating that these complexes modify the tertiary structure of pB*R*322. These electrophoretic studies indicate that the strength of the interaction of **2** to DNA (lane 3) is much larger than that of ethydium bromide (the dye). In the case of **1**, this situation is not so drastic, but nevertheless, lane 2 in Figure 10 is not as brilliant as lanes 4−6.

Atomic Force Microscopy (AFM) Study of Compound−**pB*R*322 Complexes.** AFM images of the plasmid pB*R*322 DNA incubated in the appropriate new metal complexes in concentrations corresponding to a molar ratio of $r_i = 0.005$ are shown in Figure 11. In all of the images, toroidal supercoiled forms of the plasmid DNA can be observed. These modifications are likely due to the strong effect of intercalation of the 9-aminoacridine ligand. Supercoiling in the plasmid DNA tertiary structure has been observed before for other classic intercalators such as ethydium bromide and planar heterocycles.[6,25,38] The backgrounds of the Figure 11c and d indicate the presence of a layer of water molecules from the environment over the mica surface, which can be the origin of the aggregation of the forms. In complexes **1** and **4**, a greater interaction on the DNA is observed with some formation of agglomerates.

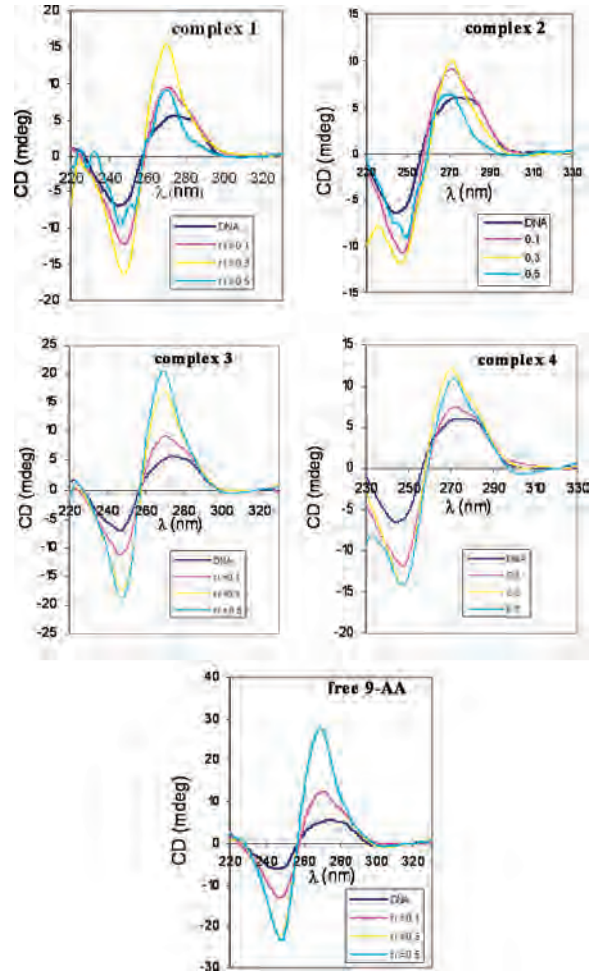

Figure 9. CD spectra of calf thymus DNA incubated with complexes **1**−**4** and free 9-AA at different r_i.

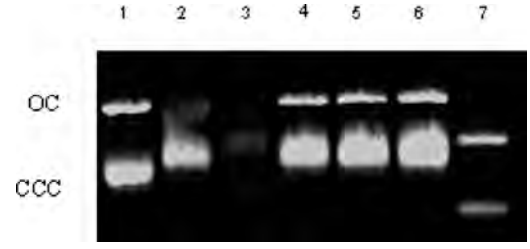

Figure 10. Electrophoretic mobility pattern of pB*R*322 plasmid DNA incubated with 9-AA and their metal complexes: lane 1, pB*R*322; lane 2, [Pd(dmba)(*N10*-9AA)(PPh_3)]ClO_4; lane 3, [Pt(dmba)(*N9*-9AA)(PPh_3)]ClO_4; lane 4, [Pd(dmba)(*N10*-9-AA)Cl]; lane 5, [Pd(C_6F_5)(*N10*-9-AA)Cl(PPh_3)]; lane 6, 9-AA; lane 7, CDDP.

When the pB*R*322 was incubated with a higher concentration of complexes **2** and **3**, a greater interaction on the DNA is observed with the formation also of aggregates in balls. Consequently, all of the new complexes modify the tertiary structure of pB*R*322, which was also observed in electrophoretic pattern.

Cytotoxicity Studies. The in vitro growth inhibitory effect of the new complexes **1**−**4** and cisplatin was evaluated in the HL-60 human tumor cell line. As listed in Table 2, both at 24 h and 72 h incubation times, all of the new complexes were more active than cisplatin. Complexes **1** and **2** are significantly more active than **3** and **4**. A possible reason might be the cationic nature of **1** and **2** that may enhance

(37) Ushay, H. M.; Tullius, T. D.; Lippard, S. J. *Biochemistry* **1981**, *20*, 3744–3748.
(38) Pope, L. H.; Davies, M. C.; Laughton, C. A.; Roberts, C. J.; Tendler, S. J. B.; Williams, P. M. *J. Microscopy* **2000**, *199*, 68–78.

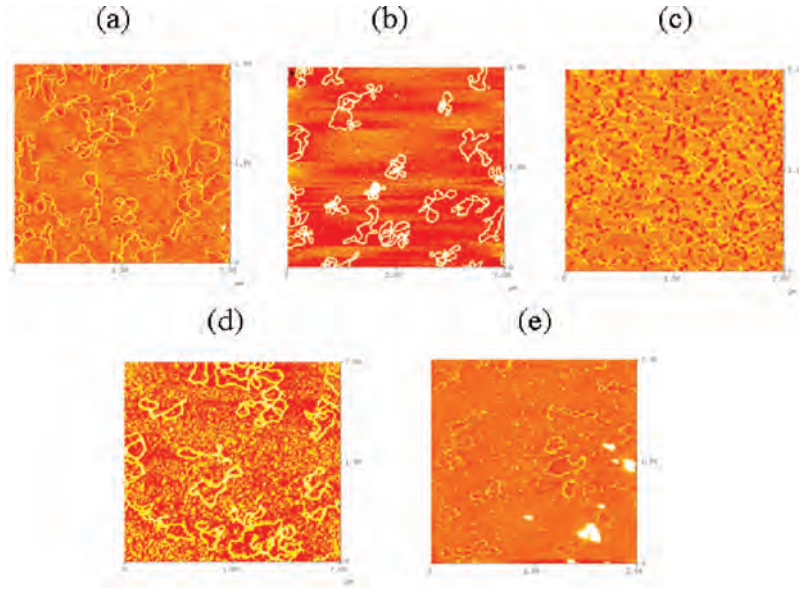

Figure 11. TMAFM image corresponding to (a) pB*R*322, (b) pBR-complex **1**, (c) pB*R*-complex **2**, (d) pB*R*-complex **3**, and (e) pB*R*-complex **4**.

Table 2. $IC_{50}(\mu M)$ for Cisplatin and Complexes **1**−**4** for the Tumor Cell Line HL-60

complex	24 h	72 h
cisplatin	15.6	2.1
1	0.52	0.45
2	0.91	0.85
3	5.92	4.64
4	6.04	4.68

their interaction with DNA (as shown in the electrophoretic studies). In fact, at a short incubation time (24 h), complex **1** was about 30-fold more active than cisplatin toward HL-60 cells.

In Vitro Apoptosis Assay. The most common and well-defined form of programmed cell death is apoptosis, which is a physiological cell suicide program that is essential for the maintenance of tissue homeostasis in multicellular organisms. In contrast to the self-contained nature of apoptotic cell death, necrosis is a messy, unregulated process of traumatic cell destruction, which is followed by the release of intracellular components. During the past decade, cell biology as well as oncology research has focused on this latter process of programmed cell death, or apoptosis. It is anticipated that an understanding of the basic mechanisms that underlie apoptosis will offer potential new targets for therapeutic treatment of diseases.[39] The type of cell death induced by the new complexes was investigated through an Annexin V/PI apoptosis assay in a flow cytometer. The results obtained for the different complexes at 24 h of incubation time were compared with those for cisplatin. With all drugs, apoptosis was observed, and the percentages are presented in Table 3.

Conclusions

Four organometallic palladium(II) and platinum(II) complexes with 9-aminoacridine have been prepared, and their crystal structures have been established by X-ray diffraction.

(39) Martin, S. J.; Green, D. R. *Curr. Opin. Oncol.* **1994**, *6*, 616–621.

Table 3. Percentages of Vital Cells, Apoptotic Cells, Dead Cells, and Damaged Cells after Treatment of a HL-60 Cell Population with Cisplatin and Complexes **1**−**4** for 24 h

treatment (IC_{50} 24 h, μM)	% vital cells (R1)	% apoptotic cells (R2)	% dead cells (R3)	% damaged cells (R4)
control	91.02	4.81	3.96	0.21
CDDP (15.6)	60.93	33.06	4.94	1.06
1 (0.52)	75.42	19.32	4.89	0.37
2 (0.91)	66.73	29.34	3.50	0.43
3 (5.92)	77.13	14.06	7.63	1.17
4 (6.04)	70.47	20.30	8.77	0.45

For palladium complexes, the ligand is coordinated in its amine form, bound to the metal atom in a monodentate fashion by the endocyclic nitrogen atom, whereas for platinum the acridine ligand adopts an imino-type configuration with the proton of the exocyclic 9-amino group shifted on N(10). In the platinum complex, an anagostic CH···Pt interaction is observed. All complexes are luminescent in the solid state at room temperature, showing important differences between the palladium and platinum complexes. The platinum complex shows two structured emission bands at high and low energies in the solid state, and the lifetimes are in agreement with excited states of triplet parentage. DFT and TD-DFT calculations for complex **2** have been done. The prediction of T_1 and T_2 excited states using TD-DFT calculations is in good agreement with those obtained in the experimental results. Values of IC_{50} were also calculated for the new complexes, **1**−**4**, against the tumor cell line HL-60. All of the new complexes were more active than cisplatin (up to 30-fold in some cases). The DNA adduct formation of the new complexes synthesized was followed by circular dichroism and electrophoretic mobility. Atomic force microscopy images of the modifications caused by the complexes on plasmid DNA pB*R*322 were also obtained.

Experimental Section

Instrumental Measurements. The C, H, and N analyses were performed with a Carlo Erba model EA 1108 microanalyzer. Decomposition temperatures were determined with a Mettler TG-

50 thermobalance at a heating rate of 5 °C min^{-1} and the solid samples under nitrogen flow (100 mL min^{-1}). The ^{1}H, ^{13}C, ^{31}P, ^{19}F, and ^{195}Pt NMR spectra were recorded on a Bruker AC 300E or a Bruker AV 400 spectrometer. Chemical shifts are cited relative to $SiMe_4$ (^{1}H and ^{13}C, external), $CFCl_3$ (^{19}F, external), 85% H_3PO_4 (^{31}P, external), and $Na_2[PtCl_6]$ (^{195}Pt, external). Infrared spectra were recorded on a Perkin-Elmer 1430 spectrophotometer using Nujol mulls between polyethylene sheets. Electrospray ionization (ESI) mass (+mode) analyses were performed on a LC-MS Agilent VL system. Excitation and emission spectra were recorded with a Jobin-Yvon Horiba Fluorolog 3-22 Tau-3 spectrofluorimeter. Phosphorescence lifetime was recorded with a Fluoromax phosphorimeter accessory containing an UV xenon flash tube with a flash rate between 0.05 and 25 Hz. The lifetime data were fitted using the Jobin-Yvon software package and the Origin 6.1 program. Solvents were dried by the usual methods.

Materials

The starting complexes [M(dmba)Cl(PPh_3)] (M = Pd and Pt),[40,41] [{Pd(dmba)(μ-Cl)}$_2$],[42] and [{Pd(C_6F_5)(PPh_3)(μ-Cl)}$_2$][43] were prepared by procedures described elsewhere. The 9-AA was purchased from Aldrich. The sodium salt of calf thymus DNA, EDTA (ethylenediaminetetraacetic acid), and Tris-HCl (tris-(hydroxymethyl)aminomethane hydrochloride) used in the CD study were obtained from Sigma (Madrid, Spain), and pB*R*322 plasmid DNA was obtained from Boehringer-Mannheim (Mannheim, Germany).

Caution! *Perchlorate salts of metal complexes with organic ligands are potentially explosive. Only small amounts of material should be prepared, and these should be handled with great caution.*

Preparation of [Pd(dmba)(*N10*-9AA)(PPh_3)]ClO_4 (1). To a solution of [Pd(dmba)Cl(PPh_3)] (100 mg, 0.19 mmol) in acetone (20 mL) was added $AgClO_4$ (39 mg, 0.19 mmol). AgCl immediately formed. The resulting suspension was stirred for 12 h and then filtered through a short pad of celite. To the filtrate was then added 9-AA (36 mg, 0.19 mmol). The solution was stirred for 24 h, and then the solvent was partially evaporated under a vacuum and hexane added to precipitate a yellow solid, which was collected by filtration and air-dried.

Data for Complex 1. Yield: 65%. Anal. calcd for $C_{40}H_{37}N_3ClO_4PPd$: C, 60.3; H, 4.7; N, 5.3. Found: C, 60.1; H, 4.9; N, 5.2. Mp: 234 °C (dec). IR (Nujol, cm^{-1}): 1642, 1618, 1574 [ν(>C=N−) and bending $\delta(NH_2)$], 1102, 624 (ClO_4), 539−492 (PPh_3). ^{1}H NMR (acetone-d_6): $\delta(SiMe_4)$ 9.41 (d, 2H, H(4) + H(5) of 9-AA, J_{HH} = 8 Hz), 8.29 (d, 2H, H(1) + H(8) of 9-AA, J_{HH} = 8 Hz), 7.92 (br, 2H, NH_2), 7.87 (m, 2H, H(3) + H(6) of 9-AA), 7.46 (br, 6H aromatic of PPh_3), 7.38 (m, 2H, H(2) + H(7) of 9-AA), 7.34 (br, 3H aromatic of PPh_3), 7.19 (d, 1H, C_6H_4 of dmba, J_{HH} = 7.2 Hz), 7.14 (br, 6H aromatic of PPh_3), 6.94 (m, 1H, C_6H_4), 6.58 (false t, 1H, C_6H_4, $J_{HH} \approx J_{HP}$ = 7.2 Hz), 6.46 (m, 1H, C_6H_4,), 4.42 (d, 2H, NCH_2 of dmba, J_{HP} = 2.4 Hz), 2.60 (d, 6H, NMe_2 of dmba, J_{HP} = 2.4 Hz). $^{13}C\{^{1}H\}$ NMR (acetone-d_6): $\delta(SiMe_4)$ 139.35 (C_6H_4 of dmba), 132.94 (CH(3) + CH(6) of 9-AA), 131.40 (aromatic CH of PPh_3), 128.37 (d, aromatic CH of PPh_3, J_{CP} = 10.6 Hz), 126.55 (CH(4) + CH(5) of 9-AA), 125.37 (C_6H_4 of dmba), 125.13 (C_6H_4 of dmba), 123.84 (CH(1) + CH(8) of 9-AA), 123.34 (CH(2) + CH(7) of 9-AA + C_6H_4 of dmba), 72.69 (CH_2NMe_2), 51.02 (NMe_2). $^{31}P\{^{1}H\}$ NMR (acetone-d_6) δ (H_3PO_4) 44.04 (s). ESI^+ mass spectra (DMSO): m/z +502.0 ([Pd(dmba)(PPh_3)]$^+$).

Preparation of [Pt(dmba)(*N9*-9AA)(PPh_3)]ClO_4·acetone (2). To a solution of [Pt(dmba)Cl(PPh_3)] (100 mg, 0.16 mmol) in acetone (20 mL) was added $AgClO_4$ (33.4 mg, 0.16 mmol). AgCl immediately formed. The resulting suspension was stirred for 12 h and then filtered through a short pad of celite. To the filtrate was then added 9-AA (31 mg, 0.16 mmol). The solution was stirred for 24 h, and then hexane was added to precipitate a yellow solid, which was collected by filtration and air-dried.

Data for Complex 2. Yield: 64%. Anal. calcd for $C_{43}H_{43}N_3ClO_5PPt$: C, 54.8; H, 4.6; N, 4.5. Found: C, 54.6; H, 4.7; N, 4.4. Mp: 188 °C (dec). IR (Nujol, cm^{-1}): 1710 [ν(>C=O), acetone] 1628, 1599 [ν(>C=N−)], 1094, 620 (ClO_4), 547−500 (PPh_3). ^{1}H NMR (acetone-d_6): $\delta(SiMe_4)$ 10.97 (d, 1H, H(1) of 9-AA, J_{H1H2} = 8.4 Hz), 10.64 (br, 1H, NH, H10), 9.16 (br, 1H, NH, H9), 7.99 (d, 1H, H(8) of 9-AA, J_{H8H7} = 8.4 Hz), 7.70 (m, 1H, H(2) of 9-AA), 7.64 (m, 6H of PPh_3), 7.41(m, 3H, H(3) + H(4) + H(5) of 9-AA), 7.31 (m, 3H of PPh_3), 7.21 (m, 8H, H(7) of 9-AA + C_6H_4 of dmba + 6H of PPh_3), 6.91 (false t, 1H, C_6H_4, $J_{HH} \approx J_{HH}$ = 7.3 Hz), 6.59 (dd, 1H, C_6H_4, J_{HH} = 7.3 Hz, J_{HP} = 2.7 Hz, J_{HPt} = 43 Hz), 6.40 (false t, 1H, C_6H_4, $J_{HH} \approx J_{HH}$ = 7.3 Hz), 4.47 (d, 1H, NCH_2 of dmba, J_{HH} = 13.6 Hz), 4.22 (dd, 1H, NCH_2 of dmba, J_{HH} = 13.6 Hz, J_{HP} = 3 Hz), 3.08 (d, 3H, NMe_2, J_{HP} = 2.4 Hz, J_{HPt} = 29 Hz), 2.91 (d, 3H, NMe_2, J_{HP} = 3.3 Hz, J_{HPt} = 25 Hz), 2.08 (s, 6H, Me_2CO). $^{13}C\{^{1}H\}$ NMR (acetone-d_6): $\delta(SiMe_4)$ 139.04 (CH(1′) of dmba), 135.32 (aromatic CH of PPh_3), 133.91 (CH(2) of 9-AA), 133.16 (CH(6) of 9-AA), 131.42 (aromatic CH of PPh_3), 128.40 (aromatic CH of PPh_3), 127.0 (CH of 9-AA), 125.3 (CH(8) of 9-AA), 124.37 (CH of dmba), 122.19 (CH of dmba), 121.59 (CH(3) of 9-AA), 117.62, 117.44 (CH(4) + CH(5) of 9-AA), 73.67 (CH_2NMe_2 of dmba), 51.41 (NMe_2), 50.84 (NMe_2), 29.5 (Me_2CO). ^{31}P NMR (acetone-d_6): δ (H_3PO_4) 20.49 (s, J_{PPt} = 4214 Hz). ^{195}Pt NMR (acetone-d_6): $\delta(Na_2[PtCl_6])$ −3930.7 (d, J_{PtP} = 4214 Hz). ESI^+ mass spectra (DMSO): m/z +784.7 ([Pt(dmba)(9AA)(PPh_3)]$^+$); 590.0 ([Pt(dmba)(PPh_3)]$^+$ −1).

Preparation of [Pd(dmba)(*N10*-9-AA)Cl]·$CHCl_3$ (3). To a solution of [Pd(dmba)(μ-Cl)]$_2$ (100 mg, 0.18 mmol) in $CHCl_3$ (20 mL) was added 9-AA (70.34 mg, 0.36 mmol). The solution was stirred for 24 h. The resulting suspension was filtered. A yellow solid was collected by filtration and air-dried.

Data for Complex 3. Yield: 90%. Anal. calcd for $C_{23}H_{23}N_3Cl_4Pd$: C, 46.9; H, 3.9; N, 7.1. Found: C, 47.6; H, 4.2; N, 7.2. Mp: 194 °C (dec). IR (Nujol, cm^{-1}): 3393, 3322, 3209 [ν(N−H)], 1637, 1609, 1566 [ν(>C=N−) and bending $\delta(NH_2)$], 358 [ν(Pd−Cl)]. ^{1}H NMR (DMSO-d_6): $\delta(SiMe_4)$ 9.47 (d, 2H, H(4) + H(5) of 9-AA, J_{HH} = 9 Hz), 8.55 (br, 2H, NH_2),), 8.46 (d, 2H, H(1) + H(8) of 9-AA, J_{HH} = 9 Hz), 8.29 (s, 1H, $CHCl_3$), 7.81 (false t, 2H, H(3) + H(6) of 9-AA, $J_{HH} \approx J_{HH}$ = 7.6 Hz), 7.41 (false t, 2H, H(2) + H(7) of 9-AA, $J_{HH} \approx J_{HH}$ = 7.6 Hz), 6.91 (d, 1H, C_6H_4 of dmba, J_{HH} = 7.2 Hz), 6.74 (false t, 1H, C_6H_4, $J_{HH} \approx J_{HH}$ = 7.2 Hz), 6.30 (false t, 1H, C_6H_4, $J_{HH} \approx J_{HH}$ = 7.2 Hz), 5.31 (d, 1H, C_6H_4 of dmba, J_{HH} = 7.2 Hz), 4.09 (s, 2H, NCH_2 of dmba), 2.95 (s, 6H, NMe_2 of dmba). $^{13}C\{^{1}H\}$ NMR (DMSO-d_6): $\delta(SiMe_4)$ 131.9 (CH of dmba), 131.4 (CH(3) + CH(6) of 9-AA), 130.4 (CH(4) + CH(5) of 9-AA), 124.5 (CH of dmba), 123.5 (CH of dmba), 123.2 (CH(1) + CH(8) of 9-AA), 122.4 (CH(2) + CH(7) of 9-AA), 121.2 (CH of dmba), 73.1 (CH_2NMe_2), 52.0 (NMe_2 of dmba). ESI^+ mass spectra (DMSO): m/z +433.8 ([Pd(dmba)(AA)]$^+$); 710.6 ([Pd$_2$(dmba)$_2$(AA)Cl]$^+$).

Preparation of [Pd(C_6F_5)(*N10*-9-AA)Cl(PPh_3)]·½$CHCl_3$ (4). To a solution of [Pd(C_6F_5)(PPh_3)(μ-Cl)]$_2$ (100 mg, 0.09 mmol) in

(40) Deeming, A. J.; Rothwell, I. P.; Hursthouse, M. B.; New, L. *J. Chem. Soc., Dalton Trans.* **1978**, 1490–1496.
(41) Meijer, M. D.; Kleij, A. W.; Williams, B. S.; Ellis, D.; Lutz, M.; Spek, A. L.; van Klink, G. P. M.; van Koten, G. *Organometallics* **2002**, *21*, 264–271.
(42) Cope, A. C.; Friedrich, E. C. *J. Am. Chem. Soc.* **1968**, *90*, 909–913.
(43) Usón, R.; Forniés, J.; Navarro, R.; García, M. P. *Inorg. Chim. Acta* **1979**, *33*, 69–75.

Table 4. Crystal Structure Determination Details

param	**1**	2·acetone	**3**·DMF	**4**·acetone·toluene
empirical formula	$C_{40}H_{37}ClN_3O_4PPd$	$C_{43}H_{43}ClN_3O_5PPt$	$C_{25}H_{29}ClN_4OPd$	$C_{47}H_{39}ClF_5N_2OPPd$
fw	796.55	943.31	543.37	915.62
cryst syst	monoclinic	monoclinic	orthorhombic	triclinic
space group	$P2_1/c$	$P2_1/c$	$Pbca$	$P\bar{1}$
a (Å)	18.3063(11)	13.8181(6)	11.7887(6)	11.6276(6)
b (Å)	9.5252(5)	14.6014(6)	11.5472(6)	12.4619(6)
c (Å)	19.8347(11)	20.0898(8)	35.4910(19)	14.5469(8)
α (deg)	90	90	90	79.679(2)
β (deg)	94.184(2)	105.367(2)	90	80.245(2)
γ (deg)	90	90	90	83.291(2)
V (Å^3)	3449.4(3)	3908.5(3)	4831.3(4)	2035.64(18)
temp (K)	100(2)	100(2)	100(2)	100(2)
Z	4	4	8	2
μ (mm^{-1})	0.710	3.749	0.903	0.623
reflns collcd	38866	42435	49656	22610
ind reflns	8031	7984	4942	8270
data/restraints/params	8031/44/519	7984/2/494	4942/0/305	8270/17/521
R (int)	0.0293	0.0285	0.0270	0.0191
R1 [$I > 2\sigma(I)$][a]	0.0410	0.0277	0.0271	0.0327
wR2 (all data)[b]	0.0983	0.0615	0.0638	0.0815
largest diff. peak and hole (e·Å^{-3})	2.301 and −0.735	0.771 and −0.528	0.569 and −0.500	0.727 and −0.638

[a] $R1 = \sum||F_o| - |F_c||/\sum|F_o|$, $wR2 = [\sum[w(F_o^2 - F_c^2)^2]/\sum w(F_o^2)^2]^{0.5}$. [b] $w = 1/[\sigma^2 - (F_o^2) + (aP)^2 + bP]$, where $P = (2F_c^2 + F_o^2)/3$ and a and b are constants set by the program.

$CHCl_3$ (20 mL) was added 9-AA (34.96 mg, 0.18 mmol). The resulting solution was stirred for 24 h. The resulting suspension was filtered to precipitate a yellow solid, which was collected by filtration and air-dried.

Data for Complex 4. Yield: 88%. Anal. calcd for $C_{37}H_{25}N_2ClF_5PPd\cdot{}^1/_2CHCl_3$: C, 54.6; H, 3.1; N, 3.4. Found: C, 54.3; H, 3.3; N, 3.4. Mp: 160 °C (dec). IR(Nujol, cm^{-1}): 3479, 3323, 3242 [ν(N−H)], 1646, 1571 [ν(>C=N−) and bending $\delta(NH_2)$], 1059, 958 (C_6F_5), 783 (Pd−C_6F_5 str), 535−500 (PPh_3), 298 ν(Pd−Cl). ^{1}H NMR (DMSO-d_6): $\delta(SiMe_4)$ 9.42 (dd, 2H, H(4) + H(5) of 9-AA, $J_{HH} = 8.4$ Hz, $J_{HP} = 2.7$ Hz), 8.53 (brs, 2H, NH_2), 8.41 (d, 2H, H(1) + H(8) of 9-AA, $J_{HH} = 8.4$ Hz), 8.30 (s, 0.5H, $CHCl_3$), 7.96 (false t, 2H, H(3) +H(6), $J_{HH} \approx J_{HH} = 7.6$ Hz), 7.74 (m, 6H of PPh_3), 7.4 (m, 9H of PPh_3), 7.43 (false t, 2H, H(2)+H(7) of 9-AA, $J_{HH} \approx J_{HH} = 7.6$ Hz). ^{19}F NMR (DMSO-d_6): $\delta(CFCl_3)$ −113.8 (m, 2F_o), −161.5 (t, 1F_p, $J_{mp} = 20$ Hz), −162.6 (m, 2F_m). ^{31}P NMR (DMSO-d_6): $\delta(H_3PO_4)$ 28.86 (t, $J_{PF} = 8$ Hz). ^{13}C{^{1}H} NMR (DMSO-d_6): $\delta(SiMe_4)$ 133.9 (d, aromatic CH of PPh_3, $J_{PF} = 10.3$ Hz), 131.3 (CH(3) + CH(6) of 9-AA), 131.0 (aromatic CH of PPh_3), 128.4 (aromatic CH of PPh_3), 128.3 (CH(4) + CH(5) of 9-AA), 123.3 (CH(1) + CH(8) of 9-AA), 122.4 (CH(2) + CH(7) of 9-AA). ESI$^+$ mass spectra (DMSO): m/z +729.0 ($[Pd(C_6F_5)(9AA)(PPh_3)]^+$); 1005.6 ($[Pd_2(C_6F_5)_2(PPh_3)(9AA)]^+$ + 1).

X-Ray Crystal Structure Analysis. Suitable crystals of **1** and **2**·acetone were grown from acetone/hexane. Crystals from **3**·DMF were grown from DMF evaporation. Crystals from **4**·acetone·toluene were grown from acetone/toluene. The crystal and molecular structures of the compounds **1**, **2**·acetone, **3**·DMF, and **4**·toluene·acetone have been determined by X-ray diffraction studies (Table 4).

The crystals were mounted onto the tip of a glass fiber, and the data collection was performed with a Bruker Smart APEX diffractometer. Data were collected using monochromated Mo Kα radiation in the ϖ scan mode. The structures of **1** and **3**·DMF were solved by direct methods and **2**·acetone and **4**·toluene·acetone by the heavy atom method. All were refined anisotropically on F^2.[44] Restraints to local aromatic ring symmetry or light atom displacement factor components were applied in some cases. The NH's were refined as free and the NH_2 as free with SADI; the methyl groups were refined using rigid groups, and the other hydrogens were refined using a riding mode.

Special Features. For compound **1**, the oxygen atoms of the perchlorate anions are disordered over two positions, 64:36%. The acridine ligand is disordered over two positions, 71:29%. The hydrogen atoms of NH_2 from the minor positions of the acridine were not included in the refinement.

For compound **2**·acetone, the acetone of solvation is disordered over two positions, ca. 53:47%. Its hydrogen atoms were not included in the refinement.

For compound **4**·acetone·toluene, the C_6F_5 ligand is disordered over two positions, ca. 53:47%. The acetone of solvation is disordered over two positions, ca. 66:34%, and its hydrogen atoms were not included in the refinement.

Computational Details for DFT and TD-DFT Calculations. The model system used in the theoretical studies of cation $[Pt(Acridinium)(PPh_3)(C_6H_4-CH_2NMe_2)]^+$ **2** was taken from the X-ray diffraction data for complex **2**·acetone. Keeping all distances, angles, and dihedral angles frozen, single-point DFT calculations were performed on both model systems. In both the ground-state calculations and the subsequent calculations of the electronic excitation spectra, the B3LYP functional[45] as implemented in TURBOMOLE[46] was used. The excitation energies were obtained at the density functional level by using the time-dependent perturbation theory approach (TD-DFT),[47–51] which is a DFT generalization of the Hartree−Fock linear response or random-phase

(44) Sheldrick, G. M. *SHELXL-97, A program for Crystal Structure Refinement*; University of Göttingen: Göttingen, Germany, 1997.
(45) (a) Becke, A. D. *J. Chem. Phys.* **1992**, *96*, 2155–2160. (b) Becke, A. D. *J. Chem. Phys.* **1993**, *98*, 5648–5652. (c) Lee, C.; Yang, W.; Parr, R. G. *Phys. Rev. Lett.* **1998**, *37*, 785.
(46) Ahlrichs, R.; Bär, M.; Häser, M.; Horn, H.; Kölmel, C. *Chem. Phys. Lett.* **1989**, *162*, 165–169.
(47) Bauernschmitt, R.; Ahlrichs, R. *Chem. Phys. Lett.* **1996**, *256*, 454–464.
(48) Bauernschmitt, R.; Ahlrichs, R. *J. Chem. Phys.* **1996**, *104*, 9047–9052.
(49) Bauernschmitt, R.; Häser, M.; Ahlrichs, R. *Chem. Phys. Lett.* **1997**, *264*, 573, and refs therein.
(50) Gross, E. K. U.; Kohn, W. *Adv. Quantum Chem.* **1990**, *21*, 255.
(51) Casida, M. E. *Recent advances in density functional methods*; Chong, D. P., Ed.; World Scientific: Singapore, 1995; Vol. *1*.

approximation method[52] In all calculations, the Karlsruhe split-valence-quality basis sets[53] augmented with polarization functions[54] were used. The Stuttgart effective core potential in TURBOMOLE was used for Pt.[55]

Biological Assays

Circular Dichroism Study. Spectra were recorded at room temperature on an Applied Photophysics Π*-180 spectrometer with a 75 W xenon lamp using a computer for spectral substraction and smooth reduction. The palladium and platinum samples ($r_i = 0.1$, 0.3, 0.5) were prepared by the addition of aliquots of each compound, from stock solutions (1 mg/mL, 4% in DMSO), to a solution of calf thymus DNA (Sigma) in a TE buffer (20 μg/mL) and incubated for 24 h at 37 °C. As a blank was used a solution of each compound in a TE buffer (50 mM NaCl, 10 mM Tris-HCl, 0.1 mM EDTA, pH 7.4). Each sample was scanned twice in a range of wavelengths between 220 and 330 nm. The drawn CD spectra are the means of two independent scans. The ellipticity values are given in millidegrees (mdeg).

Electrophoretic Mobility Study. pB*R*322 plasmid DNA of 0.25 μg/μL concentration was used for the experiments. A total of 4 μL of charge maker was added to aliquot parts of 20 μL of the complex DNA compound containing 0.7 μg DNA previously incubated at 37 °C for 24 h. The mixtures were electrophoretised in 1% agarose gel in 1× TBE buffer (45 mM Tris-borate, 1 mM EDTA, pH 8.0) for 5 h at 30 V. The gel was subsequently stained in the same buffer containing ethidium bromide (1 μg/mL) for 20 min. The DNA bands were visualized with a Typhoon 9410 Variable Mode Imager (Amersham Biosciences).

Atomic Force Microscopy. Preparation of adducts DNA-metal complexes. pB*R*322 DNA (25 μg/μL), previously heated at 60 °C, was incubated in an appropriate volume with the required metal concentration corresponding to the molar ratio $r_i = 0.005$. The complexes were dissolved in HEPES buffer (40 mM HEPES pH 7.4, and 10 mM $MgCl_2$). The different solutions as well as Milli-Q water were passed through 0.2 nm FP030/3 filters (Schleicher & Schuell GmbH, Germany) and centrifuged at 4000*g* several times to avoid salt deposits and provide a clear background when they were imaged by AFM. The reactions were run at 37 °C for 24 h in the dark.

Sample Preparation for Atomic Force Microscopy. Samples were prepared by placing a drop (3 μL) of DNA solution or DNA−metal complex solution onto green mica (Ashville-Schoonmaker Mica Co., Newport News, VA). After adsorption for 5 min at room temperature, the samples were rinsed for 10 s in a jet of deionized water of 18 MΩ cm^{-1} from a Milli-Q water purification system directed onto the surface with a squeeze bottle. They were then placed into an ethanol−water mixture (1:1) 5 times and plunged 3 times each in ethanol (100%). The samples were blow-dried with compressed argon over silica gel and then imaged in the AFM.

Imaging by Atomic Force Microscopy. The samples were imaged in a Nanoscope III Multimode AFM (Digital Instrumentals Inc., Santa Barbara, CA) operating in the tapping mode in air at a scan rate of 1−3 Hz. The AFM probe was a 125-mm-long monocrystalline silicon cantilever with integrated conical-shaped Si tips (Nanosensors GmbH Germany) with an average resonance frequency $f_o = 330$ kHz and spring constant $K = 50$ N/m. The cantilever is rectangular, and the tip radius given by the supplier is 10 nm, with a cone angle of 35° and a high aspect ratio. In general, the images were obtained at room temperature ($T = 23 \pm 2$ °C), and the relative humidity was typically lower than 40%.

Cell Line and Culture. The cell line used in this experiment was the human acute promyelocytic leukemia cell line HL-60 (American type Culture Collection). Cells were routinely maintained in a RPMI-1640 medium supplemented with 10% (v/v) heat inactivated fetal bovine serum, 2 mmol/L of glutamine, 100 U/mL of penicillin, and 100 μg/mL of streptomycin (Life Technologies, Inc.) in a highly humidified atmosphere of 95% air with 5% CO_2 at 37 °C.

Cytotoxicity Assay. The growth inhibitory effect of metal complexes on the leukemia HL-60 cell line was measured by the microculture tetrazolium [3-(4,5-dimethylthiazol-2-yl)-2,5-diphenyltetrazolium bromide, MTT] assay.[56]

Briefly, cells growing in the logarithmic phase were seeded into 96-well microtiter plates in 100 μL of the appropriate culture medium at a plating density of 1×10^4 cells/well.

Following the addition of different complex concentrations to quadruplicate wells, plates were incubated at 37 °C for 24 or 72 h. Aliquots of 20 μL of MTT solution were then added to each well. After 3 h, the color formed was quantitated by a spectrophotometric plate reader (BIO-TEK INSTRUMENTS, INC) at a 490 nm wavelength. The percentage cell viability was calculated by dividing the average absorbance of the cells treated with a palladium or platinum complex by that of the control; the percent cell viability versus drug concentration (logarithmic scale) was plotted to determine the IC_{50} (drug concentration at which 50% of the cells are viable relative to the control), with its estimated error derived from the average of three trials.

In Vitro Apoptosis Assay. The induction of apoptosis *in vitro* by the metal complexes **1**−**4** and cisplatin was determined by a flow cytometric assay with Annexin V-FITC[57] by using an Annexin V-FITC Apoptosis Detection Kit (Roche). Exponentially growing HL-60 cells in six-well plates (5×10^5 cells/well) were exposed to IC_{50} concentrations of cisplatin or complexes **1**−**4** for 24 h. Afterward, the cells were subjected to staining with the Annexin V-FITC and propidium iodide, as detailed by the manufacturer. The amount of apoptotic cells was analyzed by flow cytometry (BD FACSCalibur).

Acknowledgment. This work was supported by the Dirección General de Investigación del Ministerio de Ciencia y Tecnología (Project CTQ2005-09231-C02-01/BQU and BIO2007-6846-C02-01), Spain, and the Fundación Séneca de la Comunidad Autónoma de la Región de Murcia (Project 00448/PI/04), Spain. We thank Dr. M. J. Prieto for AFM facilities (Universitat de Barcelona) and Dr. Francisca García (Cell Culture Facility) and Manuela Costa (Cytometry Facility) for technical assistance.

Supporting Information Available: X-ray crystallography data in CIF format for complexes **1**, **2**·acetone, **3**·DMF, and **4**·acetone·toluene. This material is available free of charge via the Internet at http://pubs.acs.org.

IC800589M

(52) Olsen, J.; Jørgensen, P. *Modern electronic structure theory*; Yarkony, D. R., Ed.; World Scientific: Singapore, 1995; Vol. *2*.
(53) Schäfer, A.; Horn, H.; Ahlrichs, R. *J. Chem. Phys.* **1992**, *97*, 2571.
(54) Dunning, T. H., Jr *J. Chem. Phys.* **1994**, *100*, 5829.
(55) Andrae, D.; Haeussermann, U.; Dolg, M.; Stoll, H.; Preuss, H. *Theor. Chim. Acta* **1990**, *77*, 123–141.
(56) Mosmann, T. *J. Immunol. Methods* **1983**, *65*, 55–63.
(57) Vermes, I.; Haanen, C.; Steffensnakken, H.; Reutelingsperger, C. *J. Immunol. Methods* **1995**, *184*, 39–51.